crystals

MDPI

Article

Improving the Microstructural and Mechanical Properties of Agricultural Ploughs Through Atmospheric Plasma Spray (APS) Thermal Coatings

Fabian Cezar Lupu [1], Corneliu Munteanu [1,2,*], Bogdan Istrate [1], Gelu Ianus [1], Grigore Marian [3], Nazar Boris [3,*], Teodor Marian [3,4], Marcelin Benchea [1] and Vlad Nicolae Arsenoaia [5]

1 Mechanical Engineering Faculty, "Gheorghe Asachi" Technical University of Iasi, 700050 Iasi, Romania; fabian-cezar.lupu@academic.tuiasi.ro (F.C.L.); bogdan.istrate@academic.tuiasi.ro (B.I.); gelu.ianus@academic.tuiasi.ro (G.I.); marcelin.benchea@academic.tuiasi.ro (M.B.)
2 Technical Sciences Academy of Romania, 26 Dacia Blvd., 030167 Bucharest, Romania
3 Mechanical Engineering Faculty, Technical University of Moldova, Bd. Stefan cel Mare 168. L, MD-2004 Chisinau, Moldova; grigore.marian@if.utm.md (G.M.); marian.t@agrisolutions.md (T.M.)
4 CC "BASADORO AGROTEH" LLC, 192 Alba-Iulia, Str., 2049, MD-2071 Chisinau, Moldova
5 Agriculture Faculty, "Ion Ionescu de la Brad" Iasi University of Life Sciences, 700490 Iasi, Romania; nicolae.arsenoaia@iuls.ro
* Correspondence: corneliu.munteanu@academic.tuiasi.ro (C.M.); boris.nazar@if.utm.md (N.B.)

Abstract

This paper presents experimental investigations carried out on components belonging to agricultural plough assemblies, which undergo significant mechanical loading during soil tillage operations. Due to severe operating conditions, ploughs are subjected to abrasive wear and impact stresses, so that enhancing these properties translates into improved performance, accompanied by a lower failure rate and, consequently, reduced downtime in agricultural activity. In order to upgrade the material properties of the active parts that come into direct and sustained contact with the soil—and which are therefore most vulnerable to degradation—surface thermal coatings were applied by means of Atmospheric Plasma Spray (APS) deposition, with the aim of extending service performance and component lifespan. The mechanical properties of the deposited coatings were assessed through hardness testing (approx. 204 HV) and microscratch behaviour evaluation (COF > 1). In addition, microstructural examinations were conducted using scanning electron microscopy to characterise the surface condition following the thermal deposition process. The findings confirm that thermal coatings represent a viable technical solution, enabling not only the improvement of plough component properties, but also the possibility of reconditioning worn parts by compensating, through thermal deposition, for the material loss caused by soil-induced wear during field operation.

Keywords: microstructural properties; mechanical properties; atmospheric plasma spraying (APS); agriculture tillage; mainshare; foreshare

Check for updates

Academic Editor: George D. Verros

Received: 22 June 2026
Revised: 14 July 2026
Accepted: 17 July 2026
Published: 21 July 2026

1. Introduction

The agricultural plough ranks among the most widely used soil tillage implements in the farming sector, and its active components are subjected to considerable mechanical demands arising from continuous contact with the soil and the hard mineral particles it contains [1,2]. Throughout operational use, these working parts are simultaneously exposed to abrasive wear, impact erosion, intense friction and cyclically repeated loading, all of which contribute to the gradual deterioration of their functional contact surfaces [3]. The degradation resulting from these combined mechanisms alters the geometry of the components, increases the energy consumption of the machine and compromises the quality of the tillage work performed [4]. The accelerated pace of wear entails substantial maintenance expenditures and frequent part replacement, directly undermining the economic viability of operating such equipment [5].

The conventional materials from which plough active components are manufactured, primarily carbon steels or heat-treated alloy steels, provide a reasonable balance between deformation resistance, toughness and cost-effectiveness, yet they do not always meet the requirements imposed by working conditions in soils containing various types of abrasive particles, particularly those rich in sand or gravel, where wear phenomena intensify considerably [6,7]. In response to these limitations, research within the field of surface engineering has increasingly shifted in recent years towards advanced protective solutions designed to enhance wear resistance and extend the service life of agricultural equipment [8].

Among the modern surface coating technologies, Atmospheric Plasma Spraying (APS) has established itself as one of the most effective methods for producing coatings with enhanced hardness, thermal stability and tribological performance [9,10]. The APS deposition technique allows for the application of a broad range of materials, including metallic powders such as NiCr, CoCr and WC-Co alloys, as well as ceramic powders including Al_2O_3, ZrO_2 and Cr_2O_3, providing considerable flexibility in designing coating systems tailored to the severe demands encountered in agricultural applications [11,12]. The selection of the feedstock material has a direct bearing on the microstructure, porosity, adhesion strength and wear behaviour of the resulting coating. Also, the base material is also dependent on the characteristics of the coating material through chemical composition, particle size, etc. so that the mechanical/chemical bond between them is as strong as possible [13,14].

Furthermore, regardless of the manufacturing technologies and material improvement methods used, it is worth mentioning that an essential aspect is the corrosion resistance of agricultural components, since during operation they are exposed to both moisture and chemical agents from the soil, which justifies the use of materials such as WC, Cr, etc. [15–17].

Published studies have demonstrated that metal carbide-based coatings deposited by APS exhibit reliable abrasion resistance, making them well suited for applications involving interaction with hard mineral particles [18,19]. Ceramic coatings based on Al_2O_3 or ZrO_2 are characterised by pronounced hardness and good stability under varying thermal conditions, proving effective in regimes of intense friction and fluctuating temperatures [20,21]. Furthermore, composite coating systems that combine metallic and ceramic phases can achieve a favourable balance between stiffness, toughness and the ability to absorb mechanical impact—properties of particular importance for plough components that operate in direct contact with the soil. [22,23].

The performance of coatings produced by the APS technique is closely dependent on how precisely the process parameters are controlled, including the plasma jet temperature, the velocity at which particles reach the substrate, the carrier gas flow rate and the standoff distance at the moment of spraying [24]. Proper adjustment of these variables enables a reduction in layer porosity, an increase in coating density and improved adhesion to the base material, ultimately leading to superior behaviour under conditions of elevated mechanical loading [25,26]. The specialised literature also highlights the critical role played by the prior preparation of the substrate surface, particularly through sandblasting and degreasing, in securing a strong and durable bond between the deposited layer and the underlying base material [27].

https://doi.org/10.3390/cryst16070468

The assessment of APS coatings requires comprehensive experimental investigations covering both the determination of mechanical properties and the detailed examination of the coating microstructure. Hardness tests are required to determine the material's resistance to deformation, while microscratch tests allow for the evaluation of the deposited layer's adhesion to the base material, as well as the materials' behaviour under erosive stress [28,29]. Scanning electron microscopy (SEM) is used to analyse surface morphology, porosity distribution, microstructural defects and the overall quality of the substrate–coating interface [30,31]. The correlation of these findings allows for the identification of optimal coating configurations suited to agricultural applications, particularly for the active working components of ploughs [32].

A considerable part of published research confirms the effectiveness of APS coatings in reducing wear on agricultural components. For instance, recent investigations have shown that WC-Co coatings deposited by APS can decrease wear rates by as much as 60–80% under severe abrasive conditions [33,34]. Further studies have indicated that Al_2O_3-based ceramic coatings exhibit excellent stability under dry friction conditions, proving particularly suitable for sandy soil environments [35]. Hybrid Cr_3C_2-NiCr coatings have demonstrated high wear resistance combined with good substrate adhesion, making them a recommended choice for applications involving elevated mechanical loading [36].

Beyond performance enhancement, APS technology also offers the possibility of reconditioning worn components by restoring material lost through abrasive action, thereby contributing to an extension of the service life of agricultural equipment. Manufacturers of agricultural equipment can opt for material property enhancement technologies either to increase the performance and durability of these components, or for maintenance and reconditioning work when the components show a degree of wear beyond the limits allowed for proper functioning [37,38].

The present study investigates the mechanical and microstructural behaviour of coatings deposited by APS on agricultural plough components, employing both metallic and ceramic powders as coating feedstock materials. Figure 1 provides a concise schematic overview of the successive stages of the experimental plan, spanning from the thermal deposition process through to microstructural analysis and mechanical property determination.

Figure 1. Schematic overview of the experimental stages.

2. Materials and Methods

2.1. Materials and Sample Preparation

The experimental analyses were carried out on components belonging to the agricultural plough assembly, namely the mainshare and the foreshare. These particular components were selected on the grounds that they are the first to enter direct contact with the soil during tillage operations, being consequently exposed to severe wear, both abrasive and impact-induced. Prior to coating deposition, the chemical composition of the base material was determined using a Foundry Master Smart optical emission spectrometer (Hitachi, Tokyo, Japan), in order to establish a more accurate correlation between substrate properties and coating performance.

Two sets of specimens were prepared, corresponding to the two types of powder materials employed for thermal coating deposition:

Set 1: Mainshare and foreshare specimens coated with metallic powder WOKA 3101 (88WC-12Co), selected on account of its high wear resistance properties.

Set 2: Mainshare and foreshare specimens coated with composite ceramic powder Metco 136CP (Cr_2O_3-SiO_2-TiO_2), chosen for its high hardness, chemical stability and favourable tribological behaviour.

Prior to deposition, all specimens underwent metallographic preparation through sandblasting and alcohol degreasing to remove surface contaminants and minimise the risk of coating delamination. Sectioning to the required dimensions was performed using a Metacut 302 cutting machine (Metkon, Bursa, Turkey). For metallographic preparation, the specimens were mounted in epoxy resin using an Ecopress 52 mounting press (Metkon, Bursa, Turkey). Grinding and polishing were carried out using a Forcipol 202 machine (Metkon, Bursa, Turkey), employing abrasive papers of progressively finer grit sizes (P180–P2500) along with diamond suspensions (3 μm, 1 μm and 0.25 μm), until a flat, scratch-free mirror-like surface suitable for microstructural examination was achieved.

2.2. Thermal Spray Deposition Process

Coating deposition was performed by means of the Atmospheric Plasma Spray (APS) technique, using a SPRAYWIZARD-9MCE thermal spray system - Sulzer-Metco (Wohlen, Switzerland and Westbury, NY, USA). This equipment enables precise control over the plasma jet and particle behaviour, with powder injection carried out via a carrier gas—either argon or nitrogen, nitrogen being employed in the present case—ensuring a sufficiently high quality of the deposited layers.

During the deposition process, the feedstock powder was injected into the plasma jet, where the particles were partially or fully melted and accelerated towards the base substrate. The coatings were built up through successive passes to achieve the desired thickness while maintaining uniform coverage over the geometries of both the mainshare and foreshare components. Key process parameters—including plasma current intensity, primary and secondary gas flow rates, powder feed rate and standoff distance—were kept within the recommended operational range for each powder type, so as to ensure optimal lamellar structure formation and strong adhesion to the substrate. The main process characteristics used in producing the thermal coatings of the samples used in this paper included a spraying distance of approximately 140 mm and a plasma jet temperature of approximately 10,000–12,000 °C.

Deposition was conducted under atmospheric conditions, with substrate surfaces cleaned and degreased beforehand to promote coating adhesion to the base material. The APS process was selected owing to its versatility in depositing both metallic and ceramic materials, as well as its proven effectiveness in producing surface coatings aimed at enhancing wear resistance in agricultural applications.

https://doi.org/10.3390/cryst16070468

2.3. Microstructural Characterization and Mechanical Properties Analysis

Microstructural analyses were conducted to evaluate the morphology, homogeneity and integrity of the deposited layers. A Quattro C scanning electron microscope (ThermoFisher, Brno, Czech Republic) was employed for the examination of the following:

- The surface morphology of the coatings;
- The splat-type structure characteristic of APS deposition processes;
- The elemental distribution within the deposited layer;
- The presence of porosity or microcracks;
- The adhesion quality of the coating to the substrate.

SEM images were acquired in both secondary electron (SE) mode, for highlighting topographic surface features, and backscattered electron (BSE) mode, for revealing compositional contrast, so as to select the most representative images that best capture the surface characteristics. This dual imaging approach enabled a comprehensive assessment of layer uniformity and potential defects that could influence mechanical behaviour.

The UMTR 2M-CTR tribometer, version 1.122.245 (Campbell, CA, USA), was used for surface characterisation, and the UMT Test Viewer, CP4–2.16.93+ software was employed to assess tribological behaviour. The hardness was measured by applying a normal load of 10 N to the indenter, the indentation depth and load–displacement curves were automatically recorded by the UMT Test Viewer software. The Young's modulus was automatically calculated from the unloading segment of the curve (load–displacement curve). Microindentation was performed according to ASTM E18 standard and microscratch resistance according to ASTM D7187 standard [39,40].

Mechanical property analyses are essential for evaluating coating quality, enabling both hardness testing and the determination of scratch resistance through microscratch testing.

3. Analysis of the Base Material and Powders Used for Deposition

This section presents the materials investigated within the scope of the study: the metallic base substrate, comprising the mainshare and foreshare components of the agricultural plough assembly, along with the two powder feedstocks employed for APS deposition, namely WOKA 3101 and Metco 136CP. Chemical composition was determined by means of optical emission spectrometry (OES), while morphology and microstructure were assessed through scanning electron microscopy (SEM) coupled with energy dispersive X-ray spectrometry (EDS).

3.1. Base Material—Mainshare and Foreshare

The substrate components selected for this study are the mainshare and the foreshare of an agricultural plough, both of which are in direct and sustained contact with the soil during tillage. Their exposure to simultaneous abrasive wear, impact erosion and cyclic mechanical loading justifies the need for protective surface coatings. Chemical composition was determined using a Foundry Master Smart optical emission spectrometer (Hitachi/SpArcfire); results are summarised in Table 1.

Table 1. Chemical composition of the base material (wt.%), determined by OES spectrometry.

Component	Fe [%]	C [%]	Si [%]	Mn [%]	Cr [%]	Ni [%]	Mo [%]	V [%]	W [%]
Mainshare	78.50	1.670	0.901	1.070	0.835	13.900	0.383	0.193	>0.400
Foreshare	96.70	0.412	0.336	1.460	0.396	0.139	0.046	<0.0050	<0.0250

https://doi.org/10.3390/cryst16070468

3.1.1. Mainshare

The chemical composition reveals a complex alloying pattern characteristic of a high-alloy tool steel, specifically a wear-resistant grade designed to withstand the more severe impact loading encountered during soil tillage operations, which is consistent with the fact that this component is the first to enter contact with the soil. The presence of W, Mo and V is notable, as these elements promote the formation of stable carbides, thereby contributing to enhanced wear resistance.

SEM analyses (Figure 2) reveal a relatively uniform surface at low magnification, with few discernible surface defects. At higher magnification levels (5000×–10,000×), carbides and some inclusions become apparent within a fine and homogeneous matrix.

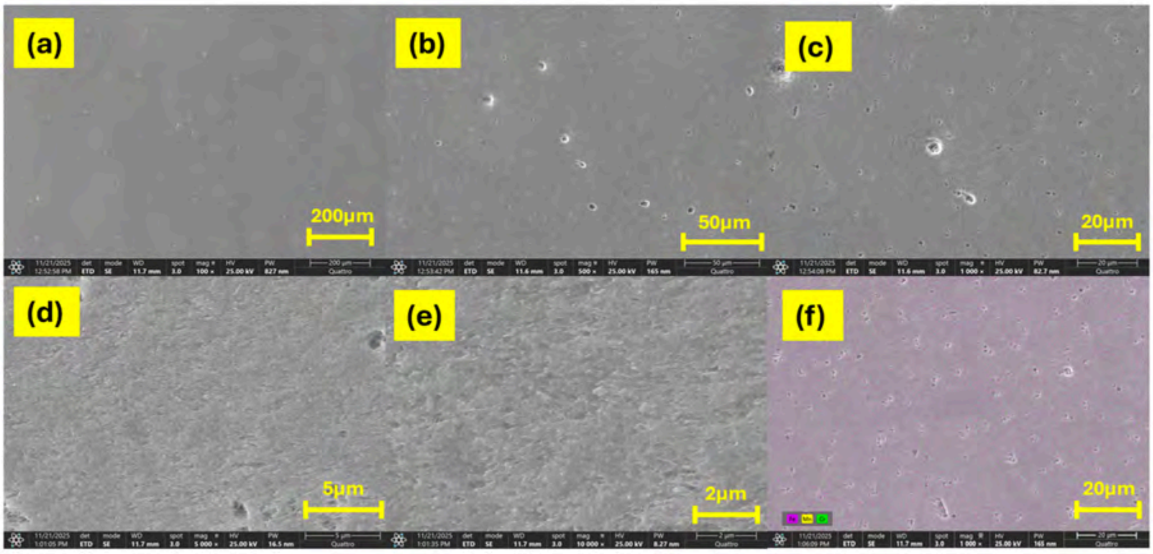

Figure 2. SEM images of the mainshare surface: (**a**) 100×, (**b**) 500×, (**c**) 1000×, (**d**) 5000×, (**e**) 10,000×, (**f**) EDS mapping.

3.1.2. Foreshare

The chemical composition is characteristic of a medium-to-low alloy carbon steel, offering a suitable balance between hardenability and toughness, with a comparatively lower carbon content relative to the other component.

SEM analyses (Figure 3) reveal a relatively uniform surface at low magnification, with some fine marks that appear to result from prior mechanical processing. Clustered microporosity and localised defects are also observable within the structure, most likely associated with the extraction of non-metallic inclusions during metallographic preparation. It is also worth mentioning that micropores are generally due to the metallurgical process of manufacturing metallic materials. Furthermore, as can be noted from the images, the surface displays a topographic contrast characteristic of a ferritic–pearlitic microstructure.

3.2. Powder Feedstocks for APS Deposition

Two commercial powders were selected for this study based on the wear resistance property requirements identified for the plough components: a WC-Co metallic powder (WOKA 3101) and a Cr_2O_3-based composite ceramic powder (Metco 136CP). Both powders were characterised by SEM/EDS prior to deposition, with the purpose of evaluating their initial condition and to support the interpretation of the microstructures of the resulting surface coatings.

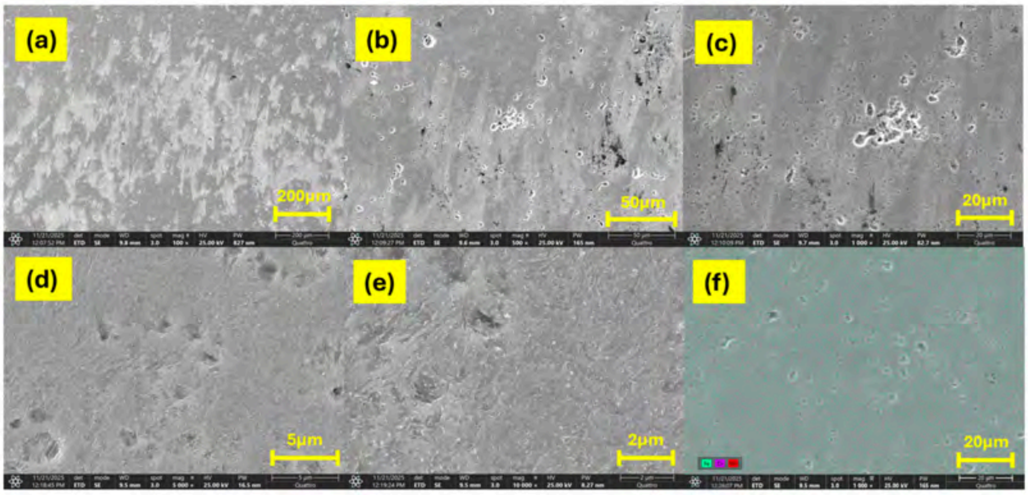

Figure 3. SEM images of the foreshare surface: (**a**) 100×, (**b**) 500×, (**c**) 1000×, (**d**) 5000×, (**e**) 10,000×, (**f**) EDS mapping.

3.2.1. Metallic Powder WOKA 3101 (88WC-12Co)

WOKA 3101 is an agglomerated and sintered cermet powder with a nominal composition of 88% WC and 12% Co. SEM examination (Figure 4) reveals predominantly spherical particles with a fine particle size distribution (approximately 16–50 μm), a morphology characteristic of the agglomeration-sintering manufacturing route, which ensures high flowability and consistent feeding behaviour during the APS process. At higher magnification levels, individual WC crystals with well-defined polyhedral structures (0.5–2 μm) can be observed, surrounded by the Co binder phase. At 5000×, spherical Co nano-precipitates are visible on the surfaces of the WC crystals, confirming a high-quality powder with a fine and uniform distribution.

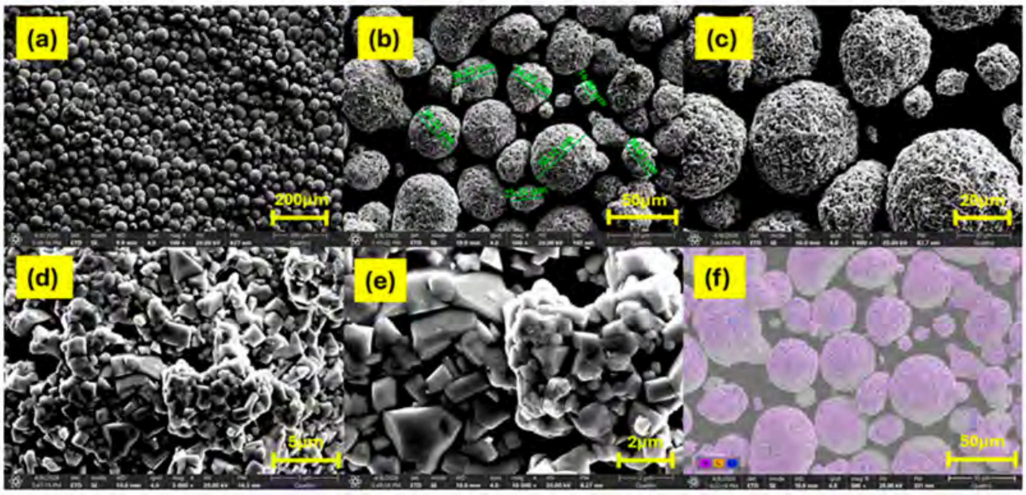

Figure 4. SEM images of WOKA 3101 powder (88WC-12Co): (**a**) 100×; (**b**) 500×; (**c**) 1000×; (**d**) 5000×; (**e**) 10,000×; (**f**) 500×—EDS mapping.

EDS analysis (Table 2) confirmed the dominant presence of W and Co, in accordance with the nominal 88WC-12Co composition. The carbon signal (38.4 at.%) is consistent with WC stoichiometry. No significant impurity elements were detected, confirming the use of a high-quality powder feedstock for APS deposition.

Table 2. EDS analysis results for WOKA 3101 powder (88WC-12Co).

Element	Line	at.%	wt.%	at.% Error	wt.% Error
C	K	38.4	4.7	0.5	0.1
Fe	K	0.2	0.1	0.1	0.1
Co	K	15.2	9.1	0.3	0.2
W	L	46.2	86.1	0.5	1.0

3.2.2. Ceramic Powder Metco 136CP (Cr_2O_3-SiO_2-TiO_2)

Metco 136CP is a composite ceramic powder based on Cr_2O_3 with SiO_2 and TiO_2 additions, intended for the production of thermally deposited coatings with high hardness, wear resistance and corrosion resistance. Unlike WOKA 3101, the particles exhibit an irregular, angular morphology with well-defined cleavage facets (Figure 5), typical of the melt-and-crush manufacturing process. The particle size distribution is considerably coarser compared to WOKA 3101, ranging from approximately 36 to over 71 µm, which may result in variable degrees of melting during plasma spraying, yielding both partially and fully molten particles. At higher magnification levels, a complex surface texture is observed, with smooth cleavage planes alternating with rougher zones, reflective of the multiphase nature of the powder.

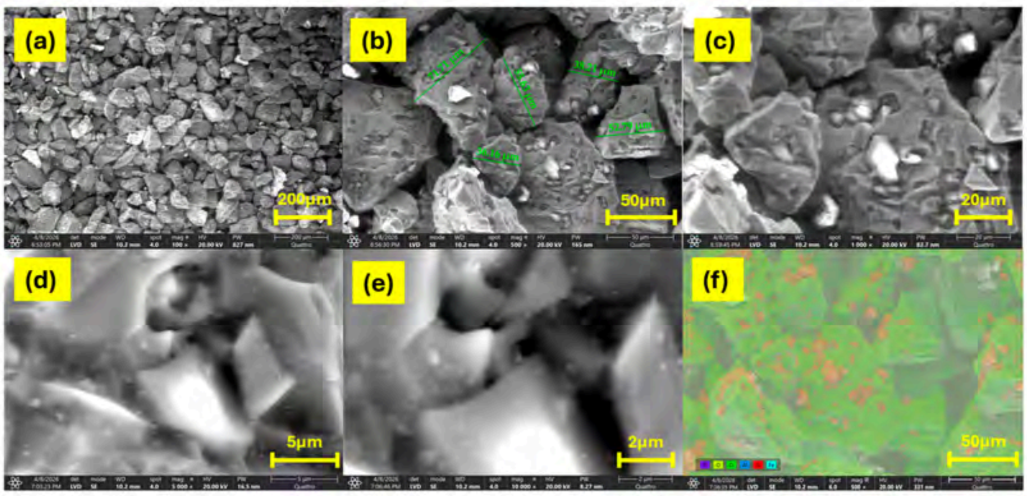

Figure 5. SEM images of Metco 136CP powder (Cr_2O_3-SiO_2-TiO_2): (**a**) 100× (**b**) 500× (**c**) 1000× (**d**) 5000×; (**e**) 10,000× (**f**) EDS mapping.

EDS analysis (Table 3) confirmed that the dominant metallic element is Cr (26.8 at.%, 50.2 wt.%), with O (59.7 at.%) consistent with the Cr_2O_3 phase. Si (8.7 at.%) and Ti (2.2 at.%) confirm the presence of the secondary SiO_2 and TiO_2 phases, while the Al signal (2.3 at.%) is attributed to trace amounts of Al_2O_3 most likely originating from the manufacturing process. The non-uniform elemental distribution at the microscopic scale is to be expected in a fused composite and does not affect the suitability of the powder for APS deposition.

Table 3. EDS analysis results for Metco 136CP powder (Cr_2O_3-SiO_2-TiO_2).

Element	Line	at.%	wt.%	at.% Error	wt.% Error
O	K	59.7	34.5	0.3	0.2
Al	K	2.3	2.2	0.0	0.0
Si	K	8.7	8.8	0.0	0.0
Ti	K	2.2	3.8	0.0	0.0
Cr	K	26.8	50.2	0.0	0.1
Fe	K	0.3	0.5	0.0	0.0

https://doi.org/10.3390/cryst16070468

The two substrate materials differ substantially in terms of chemical composition and microstructure. The foreshare is composed of a medium-to-low alloy carbon steel exhibiting a ferritic–pearlitic microstructure, whereas the mainshare is manufactured from a high-alloy steel containing significant amounts of Ni, W, Mo, Nb and V. These compositional differences are likely to influence the adhesion of the deposited coating as well as the behaviour of the interfacial bonding zone under mechanical loading.

The two powders used as feedstock materials also differ primarily in terms of morphology and composition. WOKA 3101 consists of spherical particles with a fine particle size distribution and a well-defined WC crystalline structure embedded within a Co matrix, rendering it particularly suitable for thermal deposition via the APS method. Metco 136CP, by contrast, exhibits particles of irregular shape, typical of cermet powders obtained through melting and crushing, with EDS analysis confirming a chemical composition corresponding to the Cr_2O_3-SiO_2-TiO_2 phase system.

4. Microstructural Analysis of Thermal Coatings

Both surface morphology analyses and cross-sectional analyses were carried out for all four coating-substrate combinations, designated as follows: mainshare coated with Metco 136CP (DM), mainshare coated with WOKA 3101 (DW), foreshare coated with Metco 136CP (BM) and foreshare coated with WOKA 3101 (BW). The analyses were performed using the Quattro C scanning electron microscope, with accelerating voltages ranging between 10 and 20 kV and spot sizes of up to 6. Depending on the specimen, EDS analyses were conducted on both the surface morphology and the cross-sections, in order to capture all the essential surface details.

4.1. Surface Morphology

4.1.1. Mainshare Coated with Metco 136CP

Figure 6 illustrates the surface morphology of the Metco 136CP coating deposited on the mainshare substrate material. At low magnification (100×), the coating displays a heterogeneous surface topography, comprising splats, partially molten particles and porosity, all of which represent features typical of atmospheric plasma spray (APS) deposition. The splat-on-splat layering mechanism inherent to the APS process gives rise to a rough surface with multi-scale texture. At intermediate magnification levels (500×–1000×), unmelted or partially molten spherical particles are distributed across the coating surface, with a deformed structure visible that indicates thorough thermal treatment over the course of successive plasma jet passes. A seemingly greater proportion of partially molten particles with irregular shapes is observed in comparison with the substrate of the other component analysed and presented throughout this work. At higher magnification, namely 5000×, the onset of intra-splat microcracks can be observed, some of which are fairly pronounced, indicating thermal stresses generated during the rapid solidification characteristic of the APS deposition process. At a magnification of 10,000×, agglomerations of nanoscale oxide grains can be seen at the splat boundaries, consistent with the polycrystalline Cr_2O_3 matrix.

The chemical composition obtained from EDS analysis (Table 4) confirmed chromium and oxygen as the main constituent elements, with Cr and O accounting for 33.5 at.% and 59.7 at.%, respectively, in agreement with the chromium-oxide-based composition of the Metco 136CP powder. Minor amounts of Si (3.2 at.%), Ti (2.8 at.%) and Al (0.3 at.%) correspond to the secondary oxide phases (SiO_2, TiO_2, Al_2O_3) present within the material composition. The Cr/O ratio of approximately 0.56 is close to the theoretical value of 0.67 for Cr_2O_3, confirming the integrity of the oxide phase. The low Fe signal (0.5 at.%) is most likely attributable to contamination or to a minor contribution from the substrate detected through thinner regions of the deposited layer.

https://doi.org/10.3390/cryst16070468

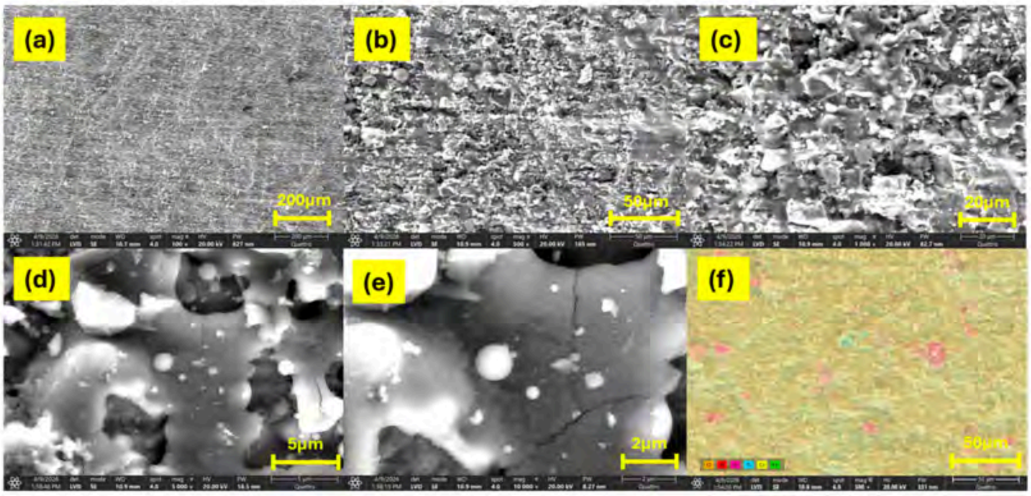

Figure 6. SEM morphology of the Metco 136CP coating surface on the mainshare substrate at (**a**) 100×, (**b**) 500×, (**c**) 1000×, (**d**) 5000×, (**e**) 10,000× and (**f**) EDS mapping.

Table 4. EDS chemical composition of the Metco 136CP coating surface on the mainshare.

Element	Linie	at. %	mas.%	at.% Error	wt.% Error
O	K	59.7	32.2	0.3	0.2
Al	K	0.3	0.3	0.0	0.0
Si	K	3.2	3.1	0.0	0.0
Ti	K	2.8	4.6	0.0	0.0
Cr	K	33.5	58.8	0.1	0.1
Fe	K	0.5	1.0	0.0	0.0

4.1.2. Mainshare Coated with WOKA 3101 (WC-Co)

The surface morphology of the WOKA 3101 (88WC-12Co) coating on the mainshare substrate is shown in Figure 7. The overall surface appearance differs markedly from that of the Metco 136CP coating, exhibiting a structure characteristic of the metallic–ceramic composite of the WC-Co system. At low magnification (100×), the coating surface displays a dense and relatively uniform texture, with apparently lower macroporosity compared with the oxide ceramic coating. At a magnification of 500×, the biphasic microstructure is composed of WC particles bound by Co, with well-defined splat boundaries indicating good coating adhesion. At higher magnification levels, fine WC particles are bound within the Co matrix, with particle sizes on the submicron scale. The images reveal a compact, well-bonded cermet microstructure, with some interlamellar microcracks or minor delamination present. Individual WC crystallites are chemically bonded, displaying a morphology characteristic of sintered powder. The nanocrystalline WC phase (observable at high magnification) can be seen within the Co matrix, confirming the fine structure of the carbide particles resulting from APS thermal deposition. The dissolution of WC into the Co phase during plasma spraying is evidenced by the diffuse boundaries between the carbide structure and the binder phase, indicating partial decarburisation, most likely due to the elevated temperatures encountered during deposition.

EDS analysis of the coating surface on the mainshare (Table 5) confirmed the WC-Co composition: W at 39.9 at.% (80.8 wt.%), Co at 21.2 at.% (13.7 wt.%) and C at 38.3 at.% (5.1 wt.%). The atomic C/W ratio of approximately 0.96 is close to the theoretical stoichiometric value of 1.0 for WC, indicating minimal decarburisation within the analysed region. The relatively low Fe content (0.6 at.%) is most likely attributable to impurity contamination. The resulting chemical composition is consistent with the nominal 88WC-12Co composition of the WOKA 3101 feedstock powder.

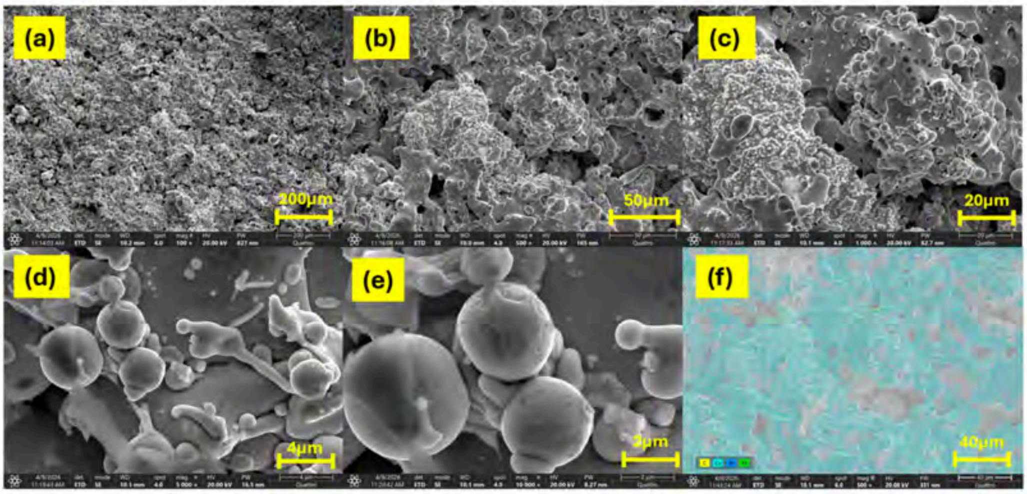

Figure 7. SEM morphology of the WOKA 3101 (WC-Co) coating surface on the mainshare substrate at (**a**) 100×, (**b**) 500×, (**c**) 1000×, (**d**) 5000×, (**e**) 10,000× and (**f**) EDS mapping.

Table 5. EDS chemical composition of the WOKA 3101 coating surface on the mainshare.

Element	Linie	at.%	mas.%	at.% Error	wt.% Error
C	K	38.3	5.1	0.3	0.0
Fe	K	0.6	0.4	0.1	0.1
Co	K	21.2	13.7	0.1	0.1
W	L	39.9	80.8	0.2	0.5

4.1.3. Foreshare Coated with Metco 136CP

The surface morphology of the Metco 136CP coating deposited on the foreshare substrate is shown in Figure 8. At low magnification (100×), the coating exhibits a heterogeneous surface topography, comprising particles deformed during deposition (splats), partially molten particles and porosity, features typical of atmospheric plasma spray (APS) deposition. The splat-on-splat layering mechanism characteristic of the APS process results in a rough surface with multi-scale texture. At slightly higher magnification (500×–1000×), unmelted or partially molten spherical particles are distributed across the coating surface, coexisting with well-deformed particles indicating complete coverage during the movement of the plasma spray gun. The general morphological characteristics are similar to those observed for the same coating on the mainshare, confirming the reproducibility of the APS deposition process across different substrate geometries. At magnification levels of 1000×–5000×, the structure likewise appears homogeneous and uniform, even though a degree of microcracking might have been expected given the brittle nature of the Cr_2O_3-SiO_2-TiO_2 ceramic system. The image acquired at 10,000× reveals the submicron-scale surface features and confirms the polycrystalline ceramic character of the coating.

EDS analysis (Table 6) confirmed the presence of substantial amounts of Cr and O, accounting for 32.1 at.% and 57.5 at.%, respectively, characteristic of the chromium-oxide-based Metco 136CP powder. The minor amounts of Si (6.1 at.%), Ti (2.4 at.%) and Al (1.6 at.%) correspond to the secondary oxide phases (SiO_2, TiO_2, Al_2O_3) present in the powder composition. The low Fe content (0.3 at.%) most likely represents an impurity.

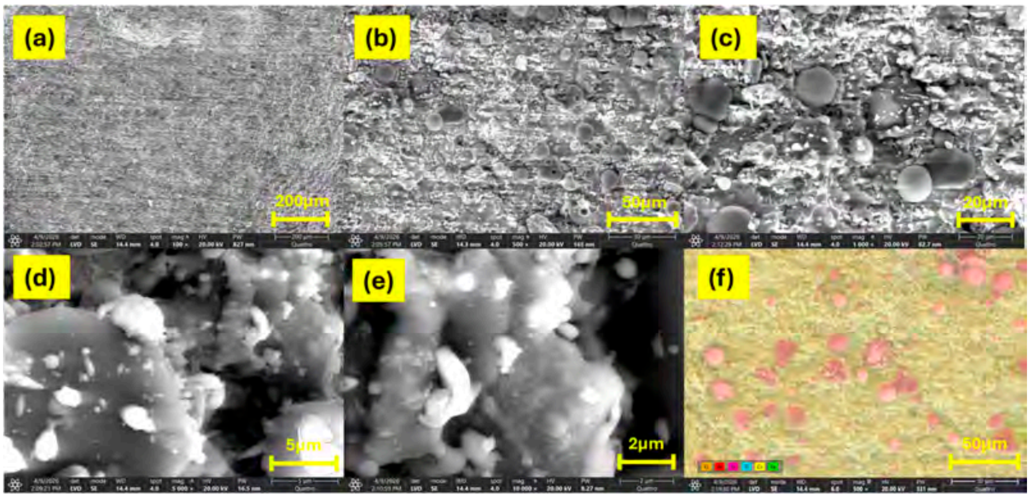

Figure 8. SEM morphology of the Metco 136CP coating surface on the foreshare substrate at (**a**) 100×, (**b**) 500×, (**c**) 1000×, (**d**) 5000×, (**e**) 10,000× and (**f**) EDS mapping.

Table 6. EDS chemical composition of the Metco 136CP coating surface on the foreshare.

Element	Line	at.%	mas.%	at.% Error	wt.% Error
O	K	57.5	31.3	0.3	0.1
Al	K	1.6	1.5	0.0	0.0
Si	K	6.1	5.8	0.0	0.0
Ti	K	2.4	3.9	0.0	0.0
Cr	K	32.1	57.0	0.1	0.1
Fe	K	0.3	0.5	0.0	0.0

4.1.4. Foreshare Coated with WOKA 3101 (WC-Co)

The surface morphology of the WOKA 3101 (88WC-12Co) coating on the foreshare is shown in Figure 9. The overall surface appearance differs markedly from that of the Metco 136CP coating, owing to the metallic–ceramic composite nature of the WC-Co system. At low magnification (100×), the coating surface displays a dense, relatively uniform texture, with apparently lower macroporosity compared with the oxide ceramic coating. At 500×, the characteristic splat-type structure consists of Co-rich deformed regions binding the embedded tungsten carbide (WC) particles, creating a complex biphasic morphology. The WC particles are embedded within a darker-contrast Co matrix, forming the typical cermet microstructure. At higher magnification levels, fine tungsten carbide particles (on the submicron scale) are bound within the Co matrix. The images reveal individual WC crystallites with sizes ranging between 0.2 and 1 μm, consistent with the morphology of the agglomerated and sintered feedstock powder. The dissolution of WC into the Co phase during plasma spraying is evidenced by the diffuse boundaries between the carbide particles and the binder, indicating partial decarburisation associated with exposure to elevated temperatures during thermal deposition, typical of the APS process.

EDS analysis of the WOKA 3101 coating surface on the foreshare (Table 7) identified W and Co as the main elements, with W at 39.5 at.% (81.1 wt.%) and Co at 19.7 at.% (13.0 wt.%). The significant atomic fraction of C (40.1 at.%) confirms the carbidic nature of the coating, corresponding to WC stoichiometry (W:C ~ 1:1). As with the other analyses, Fe impurities were identified.

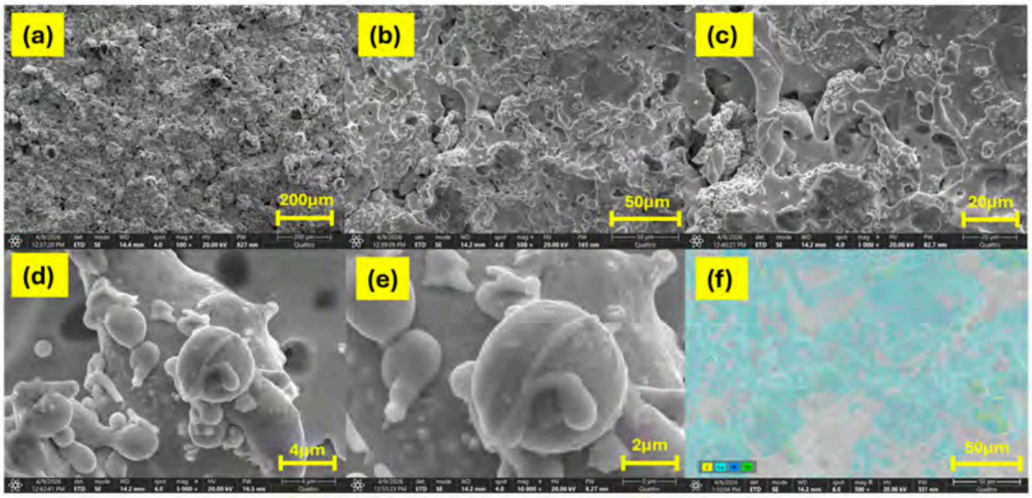

Figure 9. SEM morphological analysis of the WOKA 3101 (WC-Co) coating surface on the foreshare substrate at (**a**) 100×, (**b**) 500×, (**c**) 1000×, (**d**) 5000×, (**e**) 10,000× and (**f**) EDS mapping.

Table 7. EDS chemical composition of the WOKA 3101 coating surface on the foreshare.

Element	Line	at.%	mas.%	at.% Error	wt.% Error
C	K	40.1	5.4	0.3	0.0
Fe	K	0.7	0.5	0.1	0.1
Co	K	19.7	13.0	0.2	0.1
W	L	39.5	81.1	0.3	0.5

4.2. Cross-Sectional SEM Analysis of the Coated Specimens

Cross-sectional SEM analysis was performed on metallographically prepared specimens in order to evaluate coating thickness, internal microstructure, the quality of adhesion at the coating-substrate interface, and elemental distribution across the coating depth. For the Metco 136CP coatings, EDS analysis was carried out at 500× magnification to optimise spatial resolution given the coating thickness of approximately 30–50 µm. For the WOKA 3101 coatings, EDS analysis was conducted at 100× magnification in order to capture the entire layer thickness, which reaches higher values of approximately 300–500 µm, within a single field of view.

4.2.1. Cross-Section of the Mainshare Coated with Metco 136CP

Cross-sectional SEM images of the mainshare coating are presented in Figure 10. The image acquired at 50× magnification (Figure 10a) shows a thin, uniform ceramic layer on the steel mainshare substrate. The compositional contrast clearly delineates the coating layer from the underlying base material onto which deposition was performed. Thickness measurements indicate values ranging between 31.84 and 50.02 µm, yielding an average coating thickness of approximately 45 µm. At 500×, the cross-section reveals a splat-type microstructure characteristic of APS coatings (consistent with observations made for the other specimens), featuring bands of interlamellar porosity oriented parallel to the coating-substrate interface. The interface between the coating and the substrate exhibits moderate roughness, most likely resulting from substrate preparation through sandblasting, an operation essential for creating a surface to which the coating material can adhere. At 5000×, individual splat layers with thicknesses of 2–5 µm are clearly distinguishable, while the fine horizontal microcracks within the splats are attributed to thermal stresses generated during the rapid solidification of the molten ceramic particles. The image acquired at 10,000× reveals the network of oxide structure boundaries within the splats. The coating-substrate interface shows no signs of delamination or cracking within the bonding zone between the coating and the substrate.

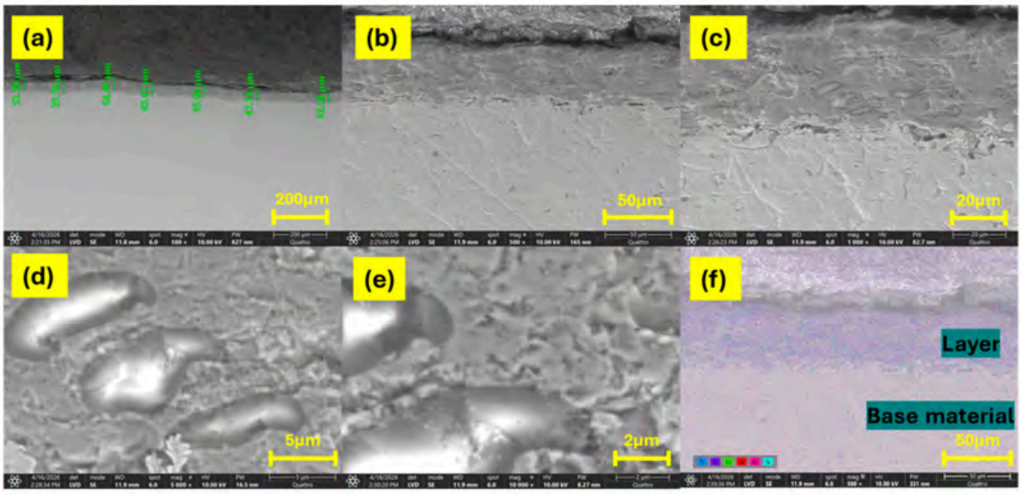

Figure 10. Cross-sectional SEM images of the Metco 136CP powder coating on the mainshare at (**a**) 100×, (**b**) 500×, (**c**) 1000×, (**d**) 5000×, (**e**) 10,000× and (**f**) EDS mapping.

The results of the EDS analysis for the mainshare cross-section (Table 8) show a high Fe content of 55.2 at.% (73.1 wt.%), which is attributable to the base material region included within the scanned area. Cr (9.8 at.%), O (30.7 at.%), Si (2.9 at.%), Ti (0.8 at.%) and Al (0.6 at.%) confirm the distribution of the Cr_2O_3-SiO_2-TiO_2 coating phase.

Table 8. EDS composition of the cross-section of the Metco 136CP coating on the mainshare.

Element	Line	at.%	mas.%	at.% Error	wt.% Error
O	K	30.7	11.6	0.3	0.1
Al	K	0.6	0.4	0.0	0.0
Si	K	2.9	1.9	0.0	0.0
Ti	K	0.8	0.9	0.1	0.1
Cr	K	9.8	12.1	0.2	0.3
Fe	K	55.2	73.1	0.7	0.9

4.2.2. Cross-Section of the Mainshare Coated with WOKA 3101

The cross-sectional analysis of the coating is presented in Figure 11. The image acquired at 50× (Figure 11a) shows the thickest coating among all four specimens examined, featuring a well-defined WC-Co layer. Thickness measurements indicate values ranging between approximately 330 and 482 µm, yielding an average coating thickness of approximately 415 µm. This represents the largest thickness recorded across all four specimen groups, suggesting that the geometry of the mainshare most likely favoured a greater accumulation of material during APS deposition. At 100× and 500×, the WC-Co microstructure appears dense and well consolidated, exhibiting relatively low porosity. The interface between the coating and the substrate is continuous and mechanically interlocked, with no signs of detachment or delamination observed. At higher magnification levels, submicron WC particles are seen to be uniformly distributed within the Co matrix, with few, insignificant pores present at the surface. The image confirms a fine cermet microstructure throughout the entire depth of the coating.

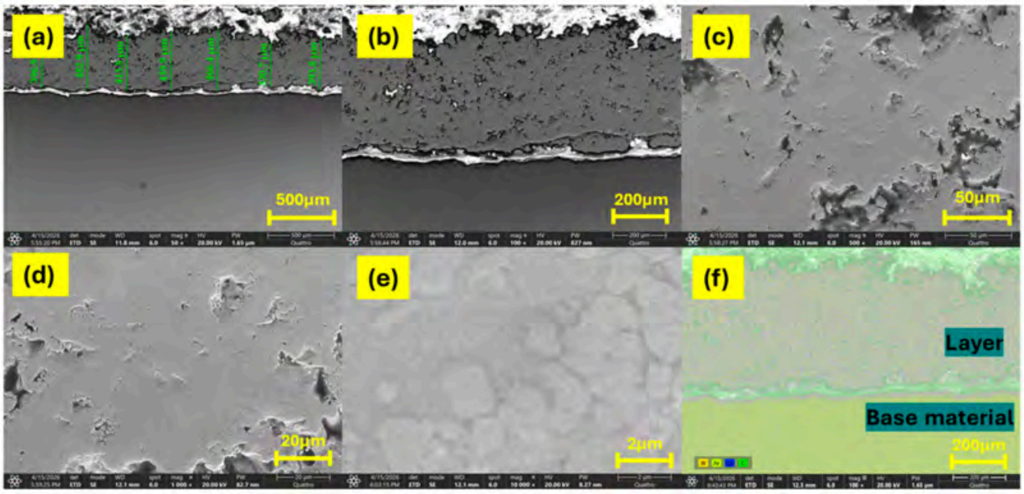

Figure 11. Cross-sectional SEM images of the WOKA 3101 coating on the mainshare at (**a**) 50×, (**b**) 100×, (**c**) 500×, (**d**) 1000×, (**e**) 10,000× and (**f**) EDS mapping.

It should be noted that, as can be observed in the SEM image, due to the metallographic grinding and polishing processing of the sample, the coating layer detaches slightly and creates a zone into which the epoxy resin from the sample mounting penetrates. This is strictly due to the metallographic processing and does not affect the good adhesion of the coating layer to the base material following the deposition process.

EDS analysis at 100× (Table 9) confirmed the WC-Co composition, comprising the following elements/percentages: C at 57.5 at.% (15.5 wt.%), W at 10.9 at.% (44.9 wt.%), Co at 3.9 at.% (5.1 wt.%) and Fe at 27.7 at.% (34.5 wt.%). The Fe content (27.7 at.%) is naturally accounted for by the fact that a substantial portion of the base material is captured within the imaged field of view. The atomic C/W ratio of approximately 5.3 within the mapped area deviates from WC stoichiometry and is attributed to background carbon contributions originating from the metallographic mounting resin included within the mapped region. Resin areas can indeed be observed at the top of the specimen in the low-magnification images.

Table 9. EDS composition of the cross-section of the WOKA 3101 coating on the mainshare.

Element	Line	at.%	mas.%	at.% Error	wt.% Error
C	K	57.5	15.5	0.3	0.1
Fe	K	27.7	34.5	0.1	0.1
Co	K	3.9	5.1	0.1	0.1
W	L	10.9	44.9	0.1	0.4

4.2.3. Cross-Section of the Foreshare Coated with Metco 136CP

Cross-sectional SEM images of the Metco 136CP powder coating on the foreshare are presented in Figure 12. At low magnification (Figure 12a), the boundary between the ceramic Cr_2O_3 coating layer and the base material substrate is fairly clearly delineated. Cross-sectional thickness measurements indicate values ranging between 29.36 and 41.76 µm, with an average coating thickness of approximately 40 µm. This value is slightly lower than that measured for the specimen coated on the mainshare (approximately 45 µm), the difference being most likely attributable to spray angle characteristics and the distribution of deposited material across the foreshare geometry. From the analysed images, the coating microstructure can be seen to be of the splat type, characteristic of the APS technique, comprising alternating layers of splats separated by fine interlamellar microporosity and horizontal microcracks running parallel to the substrate surface. At higher magnification levels, the coating-substrate interface is observed to adhere through mechanical interlocking of the ceramic splats within the asperity of the substrate surface, with no significant signs of delamination or cracking evident at the interface between the two materials.

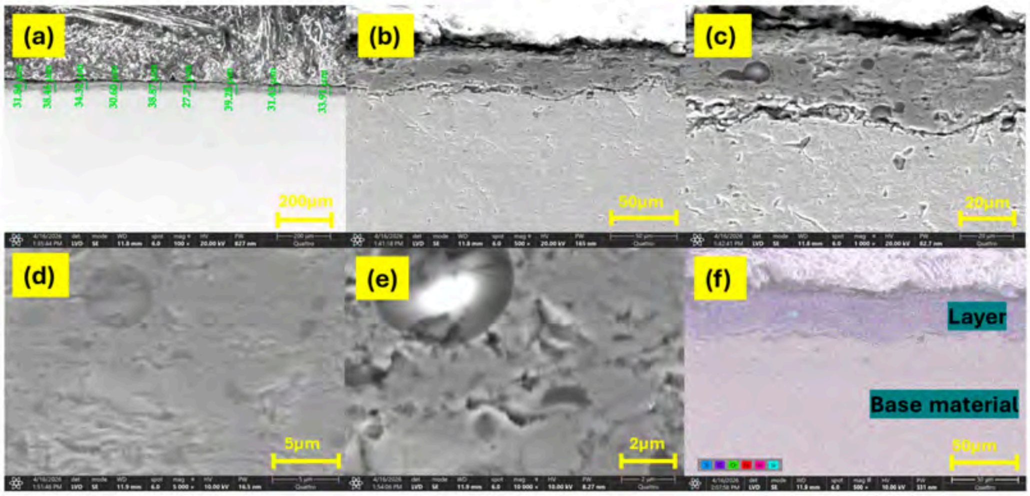

Figure 12. Cross-sectional SEM images of the Metco 136CP coating on the foreshare at (**a**) 100×, (**b**) 500×, (**c**) 1000×, (**d**) 5000×, (**e**) 10,000× and (**f**) EDS mapping.

EDS analysis of the cross-section (Table 10) shows elemental concentrations distributed as follows: Fe (68.3 at.%, 82.0 wt.%), Cr (7.5 at.%), O (21.0 at.%), Si (2.0 at.%), Ti (0.7 at.%) and Al (0.5 at.%). As with the other specimens analysed, similar observations apply here, with the high Fe content corresponding to the base material captured within the analysed region. Cr and O confirm the ceramic coating phase, while Fe, as previously noted, is entirely attributable to the base material.

Table 10. Chemical composition obtained by EDS analysis of the cross-section of the Metco 136CP coating on the foreshare.

Element	Line	at.%	mas.%	at.% Error	wt.% Error
O	K	21.0	7.3	0.2	0.1
Al	K	0.5	0.3	0.0	0.0
Si	K	2.0	1.2	0.0	0.0
Ti	K	0.7	0.7	0.1	0.1
Cr	K	7.5	8.5	0.2	0.2
Fe	K	68.3	82.0	0.7	0.9

4.2.4. Cross-Section of the Foreshare Coated with WOKA 3101

The cross-sectional analysis of the WOKA 3101 powder coating on the foreshare is presented in Figure 13. The SEM images reveal a thick, dense coating layer, clearly distinguishable from the steel substrate of the base material. The coating is uniform, of a metallic cermet WC-Co nature, exhibiting a higher average atomic number than that of the Metco 136CP ceramic coating. Cross-sectional thickness measurements indicate values ranging between 307.6 and 340.7 µm, with an average thickness of approximately 320 µm—roughly nine times thicker than the ceramic coating. This substantial coating thickness reflects the successful deposition of the WC-Co cermet system via the APS technique. SEM analyses reveal a layer microstructure composed of splats well consolidated within the base material, also exhibiting some, though insignificant, microporosity. At the coating-substrate interface, good mechanical interlocking of the coating within the substrate can be observed, with no delamination zones detected. At 500× and 10,000×, fine WC particles are homogeneously distributed within the Co phase, with few pores observed (<2 μm).

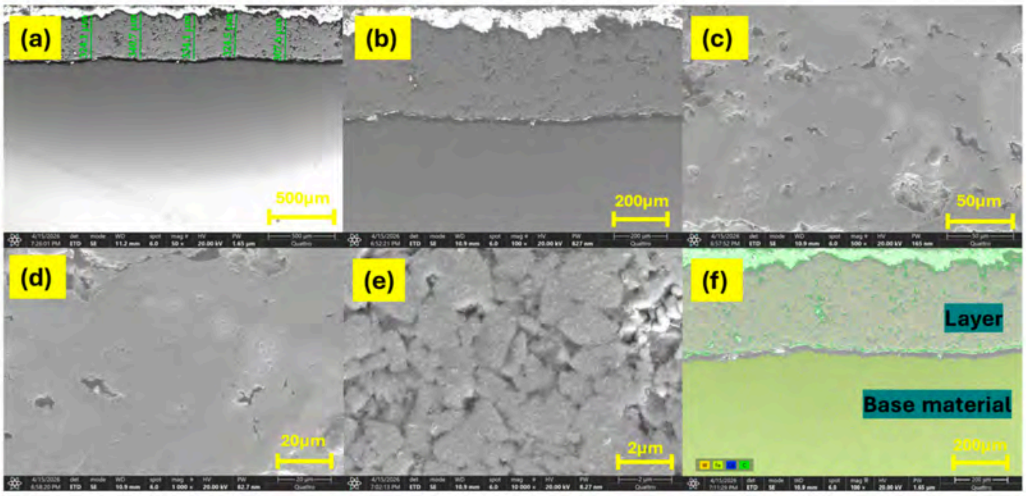

Figure 13. Cross-sectional SEM images of the WOKA 3101 coating on the foreshare at (**a**) 50×, (**b**) 100×, (**c**) 500×, (**d**) 1000×, (**e**) 10,000× and (**f**) EDS mapping.

EDS analysis at 100× (Table 11) confirmed the composition of the WC-Co coating, with values of W at 8.2 at.% (32.6 wt.%), Co at 2.4 at.% (3.0 wt.%) and C at 46.2 at.% (12.0 wt.%), while Fe accounted for 43.2 at.% (52.4 wt.%); as previously noted, this Fe content is again attributable to the base material. The presence of C confirms identification of the WC phase, and the W:Co ratio is consistent with the composition of the 88WC-12Co feedstock powder.

Table 11. EDS composition of the cross-section of the WOKA 3101 coating on the foreshare.

Element	Line	at.%	mas.%	at.% Error	wt.% Error
C	K	46.2	12.0	0.2	0.1
Fe	K	43.2	52.4	0.1	0.1
Co	K	2.4	3.0	0.1	0.1
W	L	8.2	32.6	0.1	0.3

A comparative analysis of the four coating systems reveals two distinct microstructural categories, governed primarily by the chemical composition of the powders rather than by substrate geometry. Among the two powder types, the Metco 136CP (Cr_2O_3-SiO_2-TiO_2) coatings deposited on both the mainshare and the foreshare exhibited a classical APS ceramic microstructure: thin layers (approximately 40 μm) displaying the splat-type structure characteristic of APS thermal coatings, with minor microcracking, moderate surface roughness and a heterogeneous mixture of both fully and partially molten particles. These features are well documented for plasma-sprayed oxide ceramics and stem from the high melting point of Cr_2O_3 (2435 °C), which results in complete melting of smaller particles alongside incomplete melting of larger ones. The EDS data consistently indicate Cr_2O_3 as the dominant phase (Cr: 32–34 at.%, O: 57–60 at.% in the surface analysis), with SiO_2 and TiO_2 acting as secondary phases that contribute to phase stability and enhanced wear resistance.

The WOKA 3101 (88WC-12Co) coatings, for both substrates used in deposition (mainshare and foreshare), produced substantially thicker layers (approximately 300–400 μm), denser microstructures and a characteristic morphology comprising cermet splats in which WC particles are uniformly distributed within the metallic Co matrix. The markedly lower porosity of the WC-Co coatings compared with the oxide ceramic coatings is attributed to the high deformability of Co upon impact and to the thermal conductivity properties of the cermet, which together promote stronger bonding between the splats within the structure. The partial dissolution of WC into the Co matrix, evidenced by diffuse boundaries between the carbide and the matrix, represents a phenomenon specific to WC-Co coatings deposited by the APS technique.

Both coating systems achieved good adhesion to the steel substrate of the base materials, with no evidence of layer delamination observed. Table 12 provides a comparison of the principal microstructural characteristics resulting from the SEM/EDS analyses for the four coating systems studied.

Table 12. Comparison of SEM/EDS results for the analysed coating-substrate combinations.

Samples	DM	DW	BM	BW
Coating material	Metco 136CP	WOKA 3101	Metco 136CP	WOKA 3101
Average thickness (µm)	45	400	40	300
Microstructure type	Lamellar ceramic	Cermet	Lamellar ceramic	Cermet
Surface porosity	Moderate–High	Low	Moderate	Low
Interface adhesion	Good (mechanical interlocking)	Good (mechanical interlocking)	Good (mechanical interlocking)	Good (mechanical interlocking)

5. Analysis of the Mechanical Properties of Hardness and Microscratch Resistance

The determination of mechanical properties for thermal coatings is essential in evaluating the extent to which these coatings possess the characteristics required for soil tillage applications, where elevated mechanical demands are encountered. To this end, hardness testing and microscratch testing were carried out to assess the coatings' resistance to microabrasion. The microscratch tests were performed with an increasing force from 1 N to 10 N over a distance of 10mm and for the microindentation tests, 3 determinations were made for each sample with a maximum pressing force of 10 N.

5.1. Microhardness Determination

Microhardness determination was carried out for the four specimen variants under investigation, designated as follows: B1 (foreshare coated with WOKA 3101), B2 (foreshare coated with Metco 136), D1 (mainshare coated with WOKA 3101) and D2 (mainshare coated with Metco 136). For each specimen, three measurements were performed (N1, N2, N3), with the corresponding average values presented in Table 13.

Table 13. Values obtained from the hardness determination.

Sample		B1.1	B1.2	B2.1	B2.2	D1.1	D1.2	D2.1	D2.2
Hardness [GPa]	N 1	1.544	0.830	1.334	1.293	1.145	1.329	1.926	1.889
	N 2	1.010	0.708	1.238	1.732	1.555	0.985	2.314	2.132
	N 3	1.383	1.048	1.544	1.324	0.937	0.698	1.947	1.765
	M	**1.312**	**0.862**	**1.372**	**1.450**	**1.212**	**1.004**	**2.062**	**1.929**
Young's Modulus of Elasticity [GPa]	N 1	25.144	20.738	20.753	21.311	81.991	95.742	117.977	61.302
	N 2	19.784	17.547	20.382	27.970	74.883	98.295	114.542	63.492
	N 3	20.508	22.009	21.813	24.427	68.315	110.047	115.101	56.450
	M	**21.812**	**20.098**	**20.983**	**24.569**	**75.063**	**101.361**	**115.873**	**60.415**
Stiffness (N/µm)	N 1	2.235	2.523	2.000	2.078	8.056	8.628	8.669	4.774
	N 2	2.186	2.320	2.032	2.345	6.357	10.278	7.702	4.645
	N 3	1.934	2.384	1.947	2.347	7.505	13.518	8.435	4.574
	M	**2.118**	**2.409**	**1.993**	**2.257**	**7.306**	**10.808**	**8.269**	**4.664**

Bold is used to better highlight the average measured value.

Specimen D2 (mainshare coated with Metco 136) was found to exhibit the highest average hardness value, of approximately 2 GPa, surpassing all other variants investigated. This result indicates a high resistance to local plastic deformation and suggests favourable behaviour under abrasive wear conditions.

Specimens B2 (foreshare coated with Metco 136) and B1 (foreshare coated with WOKA 3101) display comparable values of approximately 1.4 GPa and 1.3 GPa, respectively, highlighting a positive influence of the deposited layer on surface resistance.

The lowest hardness was recorded for specimen D1 (mainshare coated with WOKA 3101), with an average value of approximately 1.1 GPa.

A notable difference is observed between the foreshare and mainshare specimens. Specimens D1 and D2 exhibit elastic moduli approximately four times higher than those of specimens B1 and B2, indicating a significantly greater stiffness.

The highest stiffness was obtained for specimen D1, followed by D2. This behaviour is consistent with the elastic modulus results and highlights a greater resistance to local elastic deformation for the mainshare specimens. Figure 14 presents the indentation curves obtained from the hardness testing.

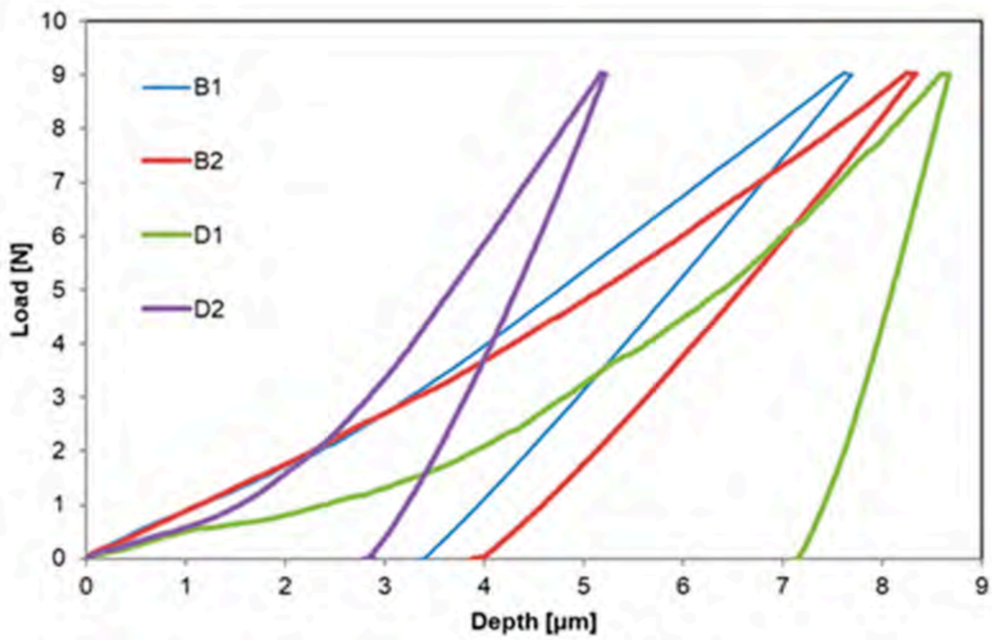

Figure 14. Graphs resulting from microhardness determination.

5.2. Determination of Microscratch Behaviour

Microscratch testing was employed to evaluate the deposited layers in terms of scratch behaviour, adhesion to the base material and progressive wear. The representative curves B1.1, B2.1, D1.1 and D2.1 were used for the comparative analysis.

The comparative graph (Figure 15) illustrates the variation in material response as a function of the load applied during the displacement of the scratching stylus.

A first assessment of the microscratch curves shows that all the specimens analysed display favourable behaviour under microscratch loading. This evaluation is based on the evolution of the apparent coefficient of friction (COF) as a function of displacement along the Y-direction, characterised by pronounced fluctuations and average values exceeding the threshold of 1. Nevertheless, a complete interpretation of scratch behaviour requires correlating the microscratch results with the microstructural observations obtained through scanning electron microscopy (SEM). In this context, specimens exhibiting scratch tracks of reduced depth and width can be regarded as more resistant to surface damage.

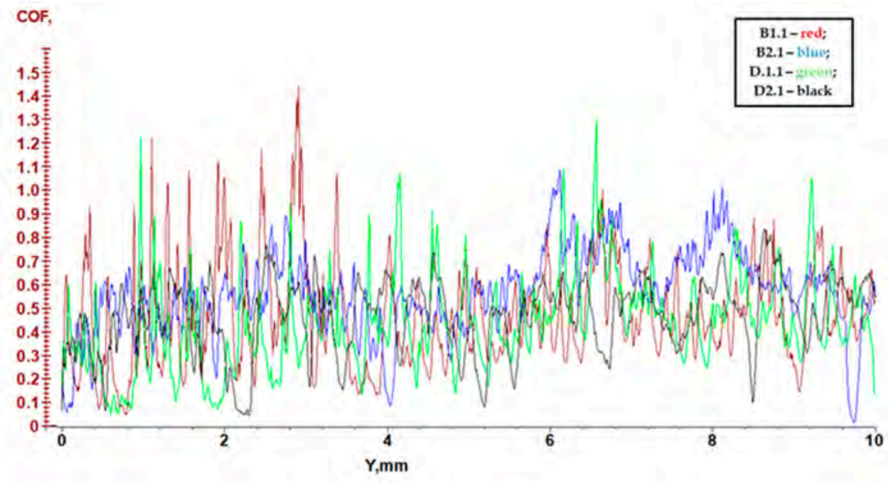

Figure 15. Graphs resulting from the microscratch tests.

As can be observed from the SEM images (Figure 16), the microscratch track widths for the four specimens are as follows:

- Foreshare coated with WOKA 3101 (B1) = 81.37 µm;
- Foreshare coated with Metco 136 (B2) = 111.05 µm;
- Mainshare coated with WOKA 3101 (D1) = 110,79 µm;
- Mainshare coated with Metco 136 (D2) = 102.80 µm.

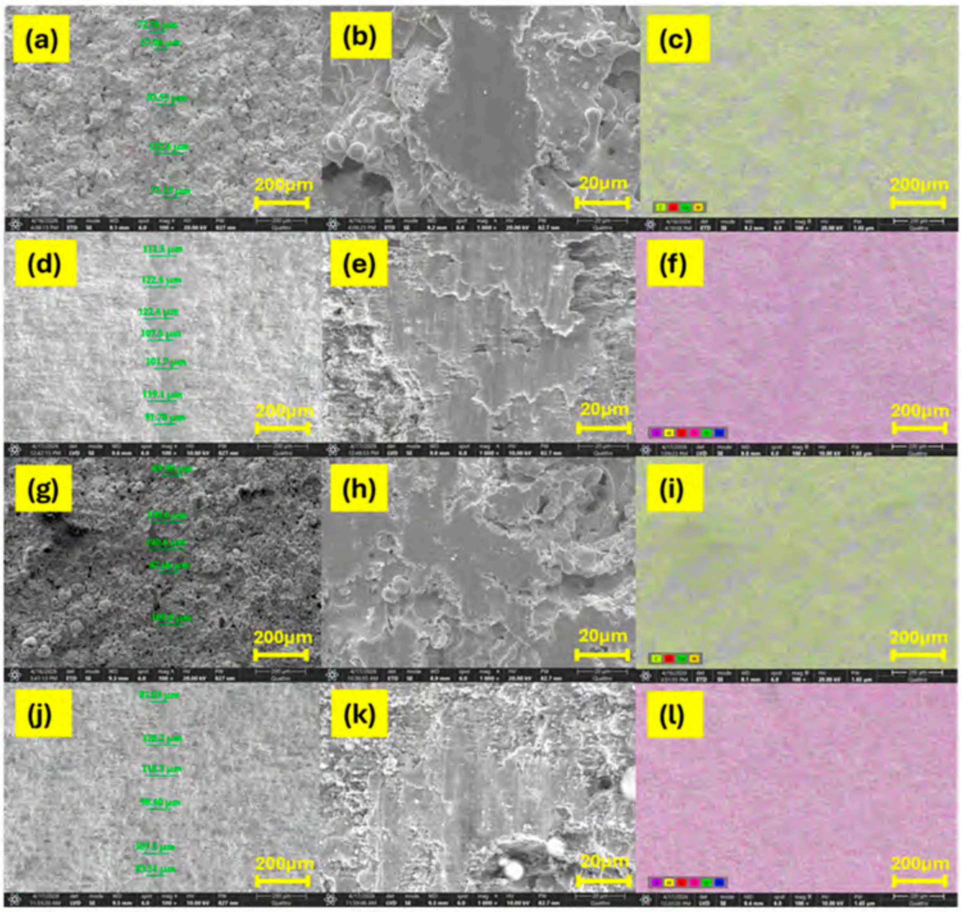

Figure 16. Microstructural images—SEM and EDS analyses: (**a**–**c**) B1 (foreshare coated with WOKA 3101), (**d**–**f**) B2 (foreshare coated with Metco 136), (**g**–**i**) D1 (mainshare coated with WOKA 3101) and (**j**–**l**) D2 (mainshare coated with Metco 136).

Based on the experimental results obtained, the following aspects can be highlighted:

all the coatings analysed exhibited high values of the apparent coefficient of friction, a behaviour characteristic of thermally sprayed layers, particularly those with a ceramic or metallic structure;

COF values exceeding 1 indicate a significant interaction between the scratching stylus and the coated surface, suggesting a good capacity for resistance to microscratching; this conclusion is further supported by the presence of repeated friction coefficient fluctuations throughout testing; all the coatings investigated demonstrated satisfactory scratch resistance, although specimen D2 (mainshare coated with Metco 136) is estimated to offer the best overall performance, owing to its superior values of microhardness, elastic modulus and stiffness as determined through microindentation testing; microstructural analyses and the elemental distribution across the specimen surfaces revealed that, for all specimens, the scratching stylus removed only the tips of the larger surface asperities of the coating layer, with the base material remaining unaffected in any region.

6. Conclusions

1. The present research investigated the mechanical and microstructural behaviour of thermal coatings produced by Atmospheric Plasma Spray (APS) deposition on agricultural plough components (mainshare and foreshare), employing two types of powders: a metallic powder (WOKA 3101, 88WC-12Co) and a ceramic powder (Metco 136CP, Cr_2O_3-SiO_2-TiO_2).
2. The chemical composition analysis of the base materials revealed substantial differences between the two components: the mainshare is manufactured from an alloy steel with a high content of Ni, W, Mo and V, favourable to the formation of stable carbides and to impact wear resistance, whereas the foreshare is made of a low alloy carbon steel with a ferritic–pearlitic microstructure and superior toughness. These substrate differences are likely to influence coating adhesion and the mechanical behaviour of the bonding zone.
3. Powder characterisation confirmed that WOKA 3101 exhibits a regular spherical morphology, with well-defined WC particles embedded in a Co matrix, ideal for the APS process, whereas Metco 136CP displays an irregular, angular morphology, typical of the melt-and-crush manufacturing process, with a coarser particle size distribution, which results in variable degrees of melting within the plasma jet.
4. Cross-sectional microstructural analysis showed that the WOKA 3101 coatings are substantially thicker (approximately 300–400 μm) than the Metco 136CP coatings (approximately 40–50 μm), as well as denser and exhibiting lower porosity, owing to the superior plastic deformation properties of the Co matrix under impact. Both coating systems exhibited good adhesion to the steel substrate, with no delamination observed, the interface being secured through mechanical interlocking, confirming the effectiveness of the prior surface preparation through sandblasting and degreasing.
5. With respect to the mechanical properties, the Metco 136 coating generally yielded higher microhardness values compared with the WOKA 3101 coating.
6. The highest average hardness was obtained for specimen D2 (mainshare coated with Metco 136), at approximately 2 GPa (approx. 204 HV), a value approximately 80% higher than that of specimen D1.
7. The mainshare specimens (D1 and D2) exhibited significantly higher elastic moduli and stiffness values than the foreshare specimens (B1 and B2), indicating a superior capacity to withstand mechanical loading.
8. The microscratch test results confirmed the trend observed in the microhardness measurements, with specimens of higher hardness displaying superior scratch resis-

tance. As can be seen in the results obtained, the coatings show high values of the apparent coefficient of friction, with values above 1, which represents good behaviour against microscratches.

9. Among all the variants investigated, specimen D2 (mainshare coated with Metco 136) exhibited the best overall combination of hardness, stiffness and microscratch resistance.

Author Contributions: Conceptualization, C.M. and F.C.L.; methodology, B.I. and F.C.L.; software, M.B. and V.N.A.; validation, G.I. and N.B.; formal analysis, G.I. and N.B.; investigation, F.C.L. and M.B.; resources, T.M.; data curation, G.I. and B.I.; writing—original draft preparation, F.C.L. and N.B.; writing—review and editing, B.I.; visualization, G.I. and V.N.A.; supervision, C.M. and G.M.; project administration, C.M. and G.M.; funding acquisition, C.M. and T.M. All authors have read and agreed to the published version of the manuscript.

Funding: This work was supported by a grant from the Ministry of Education and Research, CCCDI–UEFISCDI, project number PN-IV-PCB-RO-MD-2024-0336, within PNCDI IV.

Institutional Review Board Statement: Not applicable.

Informed Consent Statement: Not applicable.

Data Availability Statement: The data can be found at the authors of the paper.

Conflicts of Interest: Author Teodor Marian was employed by the company BASADORO AGROTEH. The re-maining authors declare that the research was conducted in the absence of any commercial or financial relation-ships that could be construed as a potential conflict of interest.

Abbreviations

The following abbreviations are used in this manuscript:

APS	atmospheric plasma spray
SE	secondary electrons
BSE	backscattered electrons
EDS	elemental distribution surface
OES	optical emission spectrometry
DM	ainshare coated with Metco 136CP
DW	mainshare coated with WOKA 3101
BM	foreshare coated with Metco 136CP
BW	foreshare coated with WOKA 3101
COF	apparent friction coefficient
B1	mainshare coated with WOKA 3101
B2	mainshare coated with Metco 136CP
D1	foreshare coated with WOKA 3101
D2	foreshare coated with Metco 136CP

References

1. Singh, J.; Chatha, S.S.; Sidhu, B.S. Abrasive wear behavior of newly developed weld overlaid tillage tools in laboratory and in actual field conditions. *J. Manuf. Processes* **2025**, *55*, 143–152. [CrossRef]
2. Yazıcı, A. Wear on steel tillage tools: A review of material, soil and dynamic conditions. *Soil Tillage Res.* **2024**, *242*, 106161. [CrossRef]
3. Zheng, X.; Sun, B.; Gao, G.; Wang, H.; Qi, Y.; Zhao, G.; Ren, J.; Zhang, Y. Tribological performance and failure mechanisms of soil-engaging components with brazed WC–Ni coatings. *Tribol. Int.* **2026**, *214*, 111139. [CrossRef]
4. Munteanu, C.; Lupu, F.C.; Istrate, B.; Ianus, G.; Marian, G.; Boris, N.; Marian, T.; Arsenoaia, V.N. Use of Thermal Coatings to Improve the Durability of Working Tools in Agricultural Tillage Machinery: A Review. *Appl. Sci.* **2026**, *16*, 474. [CrossRef]
5. Daniel, J.; Houdková, Š.; Duliškovič, J.; Grossman, J. Impact wear of the Co-based HVOF-sprayed coatings. *Tribol. Int.* **2023**, *187*, 108755. [CrossRef]

6. Dasgupta, R.; Prasado, B.K.; Modi, P.; Das, S.; Jha, A.K.; Yegneswaran, A.H. Surface engineering for improving performance of mining and agricultural implements. *Surf. Eng.* **2013**, *13*, 123–127. [CrossRef]
7. Singh, S.; Berndt, C.C.; Raman, R.K.S.; Singh, H.; Ang, A.S.M. Applications and Developments of Thermal Spray Coatings for the Iron and Steel Industry. *Materials* **2023**, *16*, 516. [CrossRef] [PubMed]
8. Liu, K.; Guo, M.; Ye, G.; Wang, Y.; Fan, W.; Du, J.; Cao, Y.; Zhang, L. Advances in plasma spraying technology for coatings: From particle flight to splat formation. *Appl. Mater. Today* **2026**, *48*, 103061. [CrossRef]
9. Guessasma, S.; Coddet, C. Microstructure of APS alumina–titania coatings analysed using artificial neural network. *Acta Mater.* **2004**, *52*, 5157–5164. [CrossRef]
10. Bozzi, A.C.; de Mello, J.D.B. Wear resistance and wear mechanisms of WC–12%Co thermal sprayed coatings in three-body abrasion. *Wear* **1999**, *233–235*, 575–587. [CrossRef]
11. Biswas, K.; Sahoo, C.K. The performance evaluation of WC/Co-Cr coating for developing hard, wear, and corrosion resistance surface using TIG arc source. *Int. J. Refract. Met. Hard Mater.* **2015**, *128*, 106983. [CrossRef]
12. Ramaiah, K.; Eswaregowda, N.B.; Tambrallimath, V.; Kuppahalli, P. Optimization of Deposition Parameters in Plasma Spray Coatings. In *Modeling and Optimization in Manufacturing: Toward Greener Production by Integrating Computer Simulation*; Wilwy: Hoboken, NJ, USA, 2021. [CrossRef]
13. Jang, B.-K.; Matsubara, H. Influence of porosity on hardness and Young's modulus of nanoporous EB-PVD TBCs by nanoindentation. *Mater. Lett.* **2005**, *59*, 3462–3466. [CrossRef]
14. Fan, T.; Liu, T.J. Micro-sliding contact problem of gradient nanostructured coating considering size effect. *Int. J. Mech. Mater. Des.* **2026**, *22*, 80. [CrossRef]
15. Kumar, V.; Singh, N.K.; Verma, R.; Mahajan, D.K.; Sharma, V.S. Corrosion behaviour of laser textured and WCCoCr+GNPs coated IS-2062 steel. *Diam. Relat. Mater.* **2023**, *136*, 109958. [CrossRef]
16. Shrivastava, S.; Kumar, V.; Verma, R.; Sharma, V. Flexural and corrosion behaviour of WC-10Co-4Cr + Graphene sprayed on textured HSLA-steel. *Surf. Eng.* **2023**, *39*, 457–472. [CrossRef]
17. Kumar, V.; Verma, R.; Kumar, R. Analysis of the corrosion and wear of WC-10Co-4Cr + GNPs coating applied to HSLA DH-36 steel using HVOF. *Surf. Topogr. Metrol. Prop.* **2022**, *10*, 045007. [CrossRef]
18. Kalemba-Rec, I.; Kopyscianski, M.; Sliwinski, P.; Dymek, S.; Węglowski, M.S.; Wrona, A. Microstructure, hardness and wear resistance of plasma-sprayed and electron beam remelted Ni-Cr-Re coatings on Inconel 625. *J. Alloys Compd.* **2025**, *1010*, 177193. [CrossRef]
19. Rats, D.; Hajek, V.; Martinu, L. Micro-scratch analysis and mechanical properties of plasma-deposited silicon-based coatings on polymer substrates. *Thin Solid Films* **1999**, *340*, 33–39. [CrossRef]
20. Iordanova, I.; Surtchev, M.; Forcey, K.S. Metallographic and SEM investigation of the microstructure of thermally sprayed coatings on steel substrates. *Surf. Coat. Technol.* **2001**, *139*, 118–126. [CrossRef]
21. Beauvais, S.; Guipont, V.; Borit, F.; Jeandin, M.; Español, M.; Khor, K.A.; Robisson, A.; Saenger, R. Process-microstructure-property relationships in controlled atmosphere plasma spraying of ceramics. *Surf. Coat. Technol.* **2004**, *183*, 204–211. [CrossRef]
22. Prasad, D.S.; Shoba, C. Hybrid composites—A better choice for high wear resistant materials. *J. Mater. Res. Technol.* **2014**, *3*, 172–178. [CrossRef]
23. Ozbek, Y.Y.; Ozgurluk, Y.; Odabas, O.; Karaoglanli, A.C. Thermal degradation resistance of HVOF-sprayed Cr_3C_2–NiCr composite coatings under oxidizing and corrosive environments. *Surf. Coat. Technol.* **2025**, *513*, 132456. [CrossRef]
24. Fei, C.; Hai, Z.; Chen, C.; Xia, Y. Study on the tribological performance of ceramic coatings on titanium alloy surfaces obtained through microarc oxidation. *Prog. Org. Coat.* **2009**, *64*, 264–267. [CrossRef]
25. Li, L.; Cao, Y.; Wang, Q.; Fan, J.; Sun, Z.; Ning, X. Microstructure, thermal and mechanical properties, and thermal cycling behavior of high-entropy $(Y_{0.2}Gd_{0.2}Er_{0.2}Yb_{0.2}Lu_{0.2})_2Zr_2O_7$/YSZ thermal barrier coatings. *Ceram. Int.* **2025**, *51*, 45581–45588. [CrossRef]
26. Tan, J.C.; Looney, L.; Hashmi, M.S.J. Component repair using HVOF thermal spraying. *J. Mater. Process. Technol.* **1999**, *92–93*, 203–208. [CrossRef]
27. Chen, X.; Dong, Z.; Wu, Y.; Si, J.; Zhang, W.; Hui, X. Multiscale ceramic–reinforced high-entropy alloy composite coating with simultaneous high resistance to sand erosion and cavitation damage. *Surf. Coat. Technol.* **2026**, *529*, 133484. [CrossRef]
28. Soltani, R.; Heydarzadeh-Sohi, M.; Ansari, M.; Afsari, F.; Valefi, Z. Effect of APS process parameters on high-temperature wear behavior of nickel–graphite abradable seal coatings. *Surf. Coat. Technol.* **2017**, *321*, 403–408. [CrossRef]
29. Duan, D.L.; Li, S.; Duan, X.H.; Li, S.Z. Wear Behavior of Thermally Sprayed Coatings under Different Loading Conditions. *Tribol. Trans.* **2005**, *48*, 45–50. [CrossRef]
30. Węglowski, M.S.; Sliwinski, P.; Dymek, S.; Kalemba-Rec, I.; Kapuściński, M.; Wrona, A.; Kustra, K. A comprehensive study on the microstructure of plasma spraying coatings after electron beam remelting. *J. Phys. Conf. Ser.* **2023**, *2443*, 012005. [CrossRef]
31. Amer, M.; Abdelgawad, A.; Curry, N.; Arshad, M.; Hayat, Q.; Janik, V.; Nottingham, J.; Bai, M. SEM-Guided Finite Element Simulation of Thermal Stresses in Multilayered Suspension Plasma-Sprayed TBCs. *Coatings* **2024**, *14*, 123. [CrossRef]

32. Munteanu, C.; Tufescu, A.; Lupu, F.C.; Istrate, B.; Benchea, M.; Melnic, I.; Vișanu, V.; Arsenoaia, V.N. Explicit FEM Analysis of Soil–Disc Interaction for APS-Coated Notched Harrow Discs in Representative Agricultural Soils. *Appl. Sci.* **2025**, *16*, 395. [CrossRef]
33. Arsenoaia, V.N.; Munteanu, C.; Lupu, F.C.; Istrate, B.; Benchea, M.; Melnic, I. Field Performance and Wear Behavior of Atmospheric Plasma Spraying (APS) Coated Discs Used in Agricultural Disc Harrows. *Agriculture* **2026**, *16*, 114. [CrossRef]
34. Suryawanshi, S.; Bhosale, D.G.; Rukhande, S.; Vasudev, H. Advanced statistical modelling of tribological performance in Ni-based thermal spray coatings: A definitive screening approach. *Results Surf. Interfaces* **2025**, *18*, 100435. [CrossRef]
35. Ram, G.P.; Karthikeyan, S.; Nicholas, P.E.; Sofia, A.S. Dry sliding wear behavior of electroless NIP and NIP-Al_2O_3 composite coatings. *Mater. Today Proc.* **2021**, *37*, 2001–2009. [CrossRef]
36. Lupu, F.C.; Munteanu, C.; Sachelarie, A.C.; Arsenoaia, V.N.; Istrate, B. Improving the usage properties of steel using cold spray deposition: A review. *Crystals* **2023**, *13*, 245. [CrossRef]
37. Singh, M.; Khan, S.W.; Anupam, A.; Singh, H.; Palanisamy, S. Sustainable recycling of waste metallic powder particles via cold spray additive manufacturing technology. *Powder Technol.* **2026**, *469*, 121915. [CrossRef]
38. Gao, R.; Huang, Y.; Zhou, X.; Ma, G.; Jin, G.; Li, T.; Wang, H.; Liu, M. Material system and tribological mechanism of plasma sprayed wear resistant coatings: Overview. *Surf. Coat. Technol.* **2024**, *483*, 130758. [CrossRef]
39. *ASTM E18*; Standard Test Methods for Rockwell Hardness and Rockwell Superficial Hardness of Metallic Materials. ASTM: West Conshohocken, PA, USA, 2017.
40. *ASTM D7187*; Standard Test Method for Measuring Mechanistic Aspects of Scratch/Mar Behavior of Paint Coatings by Nano-scratching. ASTM: West Conshohocken, PA, USA, 2020.

https://doi.org/10.3390/cryst16070468